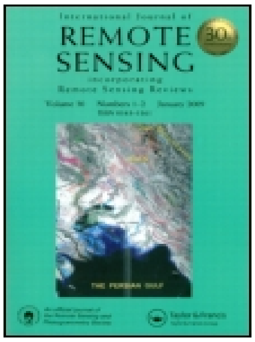

International Journal of Remote Sensing

ISSN: 0143-1161 (Print) 1366-5901 (Online) Journal homepage: http://www.tandfonline.com/loi/tres20

Review Article. The imaging of waves by satelliteborne synthetic aperture radar: the effects of sea-surface motion

M. J. TUCKER

INT. J. REMOTE SENSING, 1985, VOL. 6, NO. 7, 1059–1074

Review Article

The imaging of waves by satelliteborne synthetic aperture radar: the effects of sea-surface motion

M. J. TUCKER

Institute of Oceanographic Sciences, Crossway, Taunton, Somerset, England

(Received 1 September 1983; in final form 6 January 1984)

Abstract. The effects of sea-surface velocities in the imaging of waves by synthetic aperture radar (SAR) are considered using the 'facet' concept of the backscattering process. It is shown that if the sea wave spectrum is divided at the nominal limit of resolution of the SAR the effect of the long and short wavelength parts can be considered separately, the former being treated by numerical simulation and the latter by statistical methods. It is found that the motions due to the short wavelengths produce an azimuthal smearing which can be represented by a Gaussian low-pass filter acting on the azimuthal component of wavenumber in the image. The cut-off wavelength is typically some hundreds of metres in moderate winds. Images obtained with the SEASAT SAR frequently show such an effect.

1. Introduction

The U.S. satellite SEASAT, which operated for a few months in 1978, carried an L-band synthetic aperture radar (SAR) designed for imaging the ocean surface, and in particular for imaging surface waves. The *I.E.E.E. Journal of Oceanic Engineering* had a special issue devoted to the SEASAT sensors and this contained a paper by Jordan (1980) giving details of the SAR. The main parameters relevant to the present discussion were: altitude 800 km; radar wavelength 23·5 cm; nominal angle of incidence 20·5°; resolution on the sea surface 25 × 25 m; platform velocity in orbit 7·44 km/s; four-look integration time 0·62 s.

For those not familiar with this subject, a good review of the principles of SAR is given by Tomiyasu (1978) and the theory of the imaging of waves by microwave radars is reviewed by Alpers *et al.* (1981). Unless otherwise stated, justification for statements made below about existing knowledge will be found in these papers.

SEASAT imaged waves on many occasions. Unfortunately, corresponding surface measurements of directional wave spectra are scarce, but wavelengths and directions of travel read from optically processed images are usually in reasonable agreement with what surface information is available (see, for example, Gonzalez *et al.* 1979). However, now that more accurate images and spectra of these images are available (via digital processing), it is apparent that some process is operating which acts as a filter removing waves with high azimuthal (along-flight) wavenumbers, see, for example, Beal *et al.* (1983). It seems reasonably certain that the main cause of this azimuthal cut-off is the interaction of the surface particle velocities due to waves with the aperture synthesis process.

The concept of aperture synthesis requires the scene to be stationary during the aperture synthesis process, which took 0·62 s in the case of the SEASAT SAR four-look imagery, for example. During such a period the sea surface can move several radar wavelengths and in general this results in a degradation of the along-track (or 'azimuthal') resolution. This mechanism has been studied by Alpers (1983), who uses the deterministic equation for the SAR image of a unidirectional wave system for numerical simulation of the image assuming a unidirectional JONSWAP spectrum (Hasselmann *et al.* 1973). He simulates many realizations to get an average response (the 'Monte Carlo' technique). In the present paper we use a different approach and show that if a typical two-dimensional SAR image is considered, then the shorter wavelength sea waves can be considered separately and their effects on the response of the SAR can be calculated analytically, using established oceanographic relationships to derive the relevant statistics of sea-surface motion. 'Shorter' is defined as those wavelengths which cannot be resolved by the SAR at its nominal resolution. The effects of these are shown to degrade the azimuthal resolution by a large factor even in moderate wind speeds.

In order to reduce the complexity of the analysis, several simplifying assumptions are made.

(1) That reflections are from 'facets': that is, that they come from small uncorrelated targets which are being carried about by the water particle velocities in the waves.
(2) That the target strength of individual facets varies slowly compared with the SAR integration time.
(3) That effects due to the acceleration of the water particles can be neglected.
(4) That in the image, the spectrum of the wave modulation of the backscatter can be treated independently of the random modulation, that is, of the 'speckle'.
(5) That the sea wave system can be adequately represented by first order hydrodynamic theory.

These assumptions will be discussed briefly.

With reference to assumptions (1) and (2), the concept of a 'facet' is justified by Hasselmann *et al.* (1984), who show that on the two-scale model introduced by Wright (1968) and Bass *et al.* (1968), the reflection can be considered as coming from small patches of the sea surface, perhaps 5 Bragg resonant wavelengths across, and that in the presence of sizeable long sea waves the complex amplitudes of the reflections from these patches are uncorrelated. The 'facets' can be considered to be these patches and are therefore not sparse point targets, but sections of a continuous rough surface. This concept has been used by Alpers (1983), for example, who also assumes that the 'scene coherence time', which in this context appears to be related to the lifetime of the facets, is 10 s; for the present purpose this is long compared with the SAR integration time. Physical arguments based on the properties of the sea surface lead to a similar conclusion which can also be deduced by some rather complex analysis of published properties of the returns from a high-resolution *CW* radar.

Since a typical radar resolution cell is at least 100 Bragg wavelengths across it contains a large number of facets. This is important because later in this paper we shall be considering wavelengths that are long compared to a facet but too short to be imaged.

For the main part of the paper the effect of the phase velocity of the Bragg resonant waves which comprise the facet will be neglected. Its effect will be discussed in §5, where it will be shown to be small except in special circumstances.

With reference to assumption (3), the effects of the acceleration of the sea surface are not always negligible, but they are generally of only marginal importance and become significant in rather unusual circumstances.

With reference to assumption (4), if A is the complex target strength of a facet then, because of the properties of the sea surface, A is random in phase and amplitude in such a way that $|A|^2$ is randomly chosen from a probability distribution whose mean (or 'expected value') $|A|_e^2$ is modulated by the waves. The randomness is the 'speckle' which is a marked feature of high-resolution radar images; the modulation of the expected values of the modulus of A results in the images of the waves. When considering the two-dimensional spectrum of an image, it is possible, to first order, to consider the spectrum of the speckle and the spectrum of the modulation as independent and superimposed. Thus, in what follows we shall consider only the expected value of the radar cross-section of each facet, and ignore its random variation. This is well-established practice; Alpers and Hasselmann (1982) discuss this whole subject in detail.

Assumption (5) allows the sea wave system to be represented by the superposition of a large number of low amplitude sinusoidal wave trains travelling independently and with differing wavelengths and directions. We shall use two properties of such a system. First, on account of the random phases of the components, there is no correlation between different parts of the frequency (or wavenumber) spectrum. Secondly, since in each component wave train the water particles travel in circular orbits with a constant angular velocity, the component of this velocity along any direction (in particular the radar range direction) varies sinusoidally with time. Thus, the range component of velocity of a facet on the sea surface is the superposition of a large number of sinusoidal components with random phases and is therefore a random Gaussian variable (see, for example, Cartwright 1962.)

The mechanisms by which waves modulate the backscatter are not well understood. Some are discussed by Alpers *et al.* (1981), but since that paper was written it has become apparent that these cannot adequately explain measured data. It seems likely that variation in the surface velocity of the wind at various points on the wave profile also influences the modulation and there may be other effects. However, for the present paper we shall start with the field actually backscattered from the sea surface (equivalent to taking an instantaneous radar 'snap-shot') and examine the way its spatial spectrum is changed by the interaction of wave particle velocities and the aperture synthesis process.

It will be argued that the whole process can be regarded as three separate stages. First, the production of the primary backscattered field, as discussed above. This is then acted upon by the effects of the interaction of the surface velocity with the aperture synthesis process to produce a notional secondary scattered field. The final image is then produced by the SAR acting on this secondary scattered field as though it were stationary, which is a well-understood process. The validity of this division is assumed by Beal *et al.* (1983), for example, who define the overall system transfer function from the sea wave spectrum to the SAR image spectrum as $F(\mathbf{k})$ given by

$$F^2(\mathbf{k}) = G^2(\mathbf{k}) H^2(\mathbf{k}) J^2(\mathbf{k}) \quad (1)$$

where $G^2(\mathbf{k})$ is the 'stationary' scatter portion of $F^2(\mathbf{k})$, $H^2(\mathbf{k})$ is the moving ocean scatterer response and $J^2(\mathbf{k})$ represents the effects of the various wave imaging mechanisms.

At first glance this formulation appears to assume that the motion effects can be represented by a linear spatial filter, whereas the numerical simulations of Alpers (1983) shows that the processes are complex and non-linear. The main contribution of the present paper is to show that the motion effects can be separated into two components, one of which can indeed be treated as a linear filter. This has some important implications which will be discussed later. The other (non-linear) component is not treated in this paper.

The author has already published a brief account of some of his ideas on the subject (Tucker 1983). The present paper takes these further, together with analytical and empirical justification.

Ouchi (1982) also examines this problem using a rather similar 'facet' concept. He assumes that the backscattering is due to Bragg scatters whose amplitude and phase fluctuate randomly in space and time. The space scale is small compared with a resolution cell, as we assume here, but the time scale is small compared with the SAR integration time which is the opposite of what we assume here. However, he does not relate these fluctuations to physical processes and so is unable to quantify them.

2. The imaging process: general discussion

2.1. *The linearity of some important aspects*

The aperture synthesis process is linear in the sense that the law of superposition applies; if another target is added to the scene, it passes through the aperture synthesis process without affecting the imaging of the original targets present. If there is already another target in the same resolution cell, the complex amplitudes will add. Thus, the signals from the facets will all pass through the aperture synthesis process independently and can be added in its output before the detector stage.

Each facet is being transported by the particle velocity due to the orbital motion in the longer waves present. If v_r is the range component of velocity, then it results in an apparent along-track ('azimuthal') offset χ given by

$$\chi = (R_s/V_s) v_r \quad (2)$$

where R_s is the range and V_s is the platform velocity. (The explanation for this can be found in Tomiyasu (1978).)

This again is a linear equation, so that if

$$v_r = v_1 + v_2$$

where v_1 and v_2 are due to different components of the wave spectrum, we can write

$$\chi = \chi_1 + \chi_2 \quad (3)$$

where

$$\chi_1 = (R_s/V_s) v_1$$

and

$$\chi_2 = (R_s/V_s) v_2$$

Thus, in so far as velocity effects are concerned, the various components of the sea wave spectrum can be carried through this stage independently. One of the most useful conclusions of the present paper results from examining the statistics of χ.

In the final detection stage, the amplitudes of the signals from the facets which have finished up in a given resolution cell are added vectorially. The resultant $|\text{amplitude}|^2$ is taken as being proportional to the scattering cross-section of that resolution cell, though the vector resultant can be presented in other ways.

2.2. *Separation of the effects of small-scale and large-scale motions*

We shall temporarily consider the image as being divided into discrete sharp-edged resolution cells.

Taking account of the linear superposition of velocity effects discussed in §2.1, the velocity offset process can be considered in two stages as shown in figure 1. In the first, the facets within a resolution cell all move the same distance azimuthally due to the mean range component of velocity of the cell. In the second, they scatter due to the relative motions within the cell.

The first process can be a mechanism for imaging low-amplitude swell. This is shown diagrammatically in figure 2 and is known as 'velocity bunching'. The within-cell motions will be shown to produce a very significant smearing of the spectrum, removing components with short wavelengths in the azimuthal direction.

2.3. *Summary*

The imaging process can be considered as a series of independent steps.

(1) The primary scattered field can be considered as that produced by facets whose target strengths are constant during the SAR integration period. The expected value of the target strengths of these facets is modulated by factors such as wave slope and hydrodynamic modulation to give the primary scattered field.

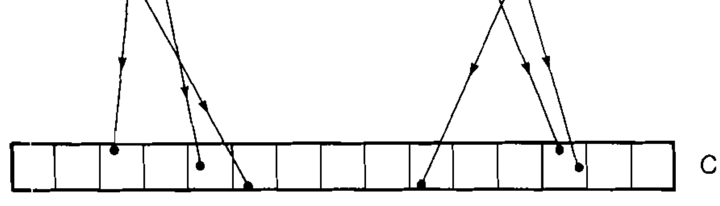

Figure 1. Azimuthal offsets due to the range components of the sea-surface velocities can be considered in two stages. A is one range cell of the primary scattering field. This is transformed to a notional scattering field B by the velocities of the cells as a whole, and into the final image by adding the effects of within-cell motions.

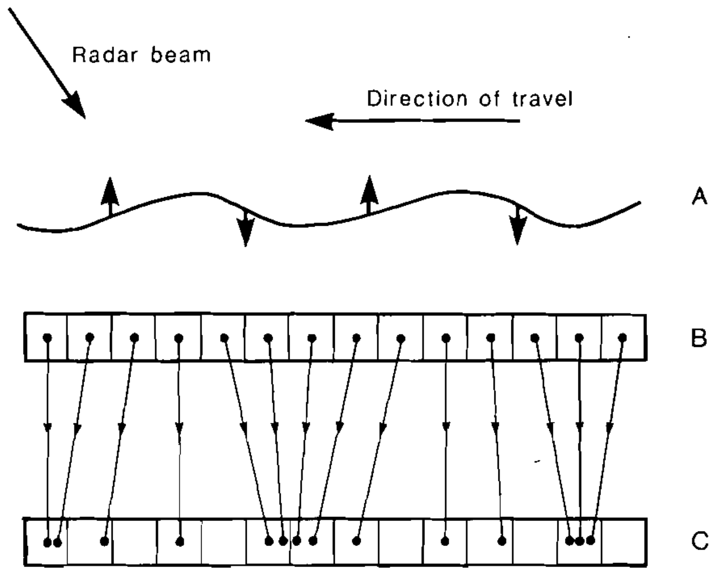

Figure 2. Sketch to show how velocity bunching can image a low swell. A is a vertical cross-section of the swell showing surface velocities. B is a plan view of one range cell. The scattering due to each resolution cell is moved azimuthally by the aperture synthesis process to give the image C, where the scattering is bunched.

(2) This field is then operated on by the azimuthal offsets caused by the range velocity component of the resolution cells as a whole, which may produce further wave modulation by the velocity bunching effect.
(3) This field is then smeared azimuthally by the within-cell motion effects.
(4) This field is then acted upon by the stationary target response of the radar.

3. The effects of small-scale motions

3.1. *Separation of motion scales in terms of the wave spectrum and its application to numerical simulation*

It is more convenient to divide the space scales of motion in terms of the wavenumber spectrum, since with the first-order assumption that waves are a stationary random Gaussian process, the various spectral components are uncorrelated. If, for example, we divide the spectrum into two parts at a wavenumber above which none of the components are imaged, the azimuthal offsets due to the high wavenumber components will be uncorrelated with the imaged components and can therefore be treated as random.

3.2. *The effect of small scale velocities: the basic theorem*

Define the image intensity variation of a particular pixel centred on x, y as

$$s(x,y)=[\sigma(x,y)-\sigma_0]/\sigma_0$$

where σ_0 is the ensemble average of $\sigma(x,y)$ over the scene and x is the azimuthal direction. $s(x,y)$ over a large rectangular scene can be considered as the sum of sinusoidal harmonics (the Fourier theorem),

$$s(x,y)=\sum_l \sum_m A_{lm} \exp\{i(k_l x+k_m y)\} \tag{4}$$

where A_{lm} is the complex amplitude of that harmonic which has l complete wavelengths in the x dimension of the scene and m complete wavelengths in the y dimension, and k_l and k_m are the corresponding wave numbers.

The next point can be made most clearly by temporarily considering $s(x,y)$ as being an actual digital radar image, so that $s(p,q)$ is available for the pixel in the pth column and qth row, the unit of distance being taken as the pixel spacing. Then the Fourier transform of the image is

$$A_{lm}=1/N\sum_p\sum_q s(p,q)\exp\{-i(k_lp+k_mq)\} \qquad (5)$$

where $N=p_{\max}q_{\max}$. This equation shows that the amplitude of a given frequency component is a weighted average of all the pixel intensities in the image. In a typical transformed scene (see §4) there are about 10^5 pixels, but the final spectral estimates may be based on the average of the transforms of a number of such scenes, and the number of pixels finally involved is typically of the order of 10^6. Thus, if we are considering effects which are random with respect to the l,mth harmonic (that is, uncorrelated with it) and whose space scale is comparable with a pixel dimension, we can treat them on a probability basis.

Suppose now that equations (4) and (5) refer to a primary scattered field, and consider notionally that it consists of small pixels with a spacing of η in both dimensions, each pixel containing one facet. If the azimuthal offset due to range velocity is χ, which is assumed to be generally fairly large compared with η, the proportion of pixels which are offset in such a way that their new centres fall within the pixel which has its centre n pixels away (along the x axis) from the original position is $p(\chi_n)\eta$, where $p(\chi)$ is the probability density function of χ and $\chi_n=n\eta$.

The offsets we are concerned with here are uncorrelated with the longer-wave components (see §1). Therefore, so far as these long waves are concerned this particular set of pixels is a random selection from the primary scattered field. It therefore has the same Fourier transform, but with its amplitude weighted by the number of pixels involved and its phase changed by an amount corresponding to a move of χ_n along the x axis. If $\Delta A'_{lm}$ is its contribution to A'_{lm}, a harmonic of the SAR-processed field, then

$$\begin{aligned}\Delta A'_{lm}&=p(\chi_n)\eta(1/N)\sum_p\sum_q s(p,q)\exp\{-i(k_l(p\eta+\chi_n)+k_mq\eta)\}\\&=p(\chi_n)\eta[\exp\{-ik_l\chi_n\}]A_{lm}\end{aligned}$$

Since η is the interval of χ corresponding to this contribution to A'_{lm} this can be converted to an integral

$$A'_{lm}\to A_{lm}\int_{-\infty}^{\infty}p(\chi)[\exp\{-ik_l\chi\}]\,d\chi$$

Or, using the symbol k_x instead of k_l, the amplitude response function of the aperture synthesis process is

$$R(k_x)=A'_{lm}/A_{lm}=\int_{-\infty}^{\infty}p(\chi)[\exp\{-ik_x\chi\}]\,d\chi \qquad (6)$$

Before evaluating this integral it is necessary to show that the spatial correlation of the velocity field due to the short wavelength part of the spectrum falls off on a scale of the order of the radar resolution. From oceanographic knowledge (see below) we can state that the wavenumber bandwidth Δk of the wave spectrum above a cut-off wavenumber k_c will be a large fraction of k_c if this part of the spectrum is saturated or near saturation, and a well-known theorem in the time domain (that $\tau \simeq 1/\Delta f$) can be converted into the space domain to give the correlation distance as approximately $2\pi/\Delta k \simeq 2\pi/k_c \simeq \lambda_c \simeq 2\rho$. Thus, there is a very large number of effectively independent offsets in the scene, as discussed earlier in this section.

3.3. *The evaluation of the response function*

Using equation (2) and the assumption that v_r is a random Gaussian variable (see §1), the azimuthal offset is

$$p(\chi) = [1/v\sqrt{(2\pi)}] \exp\{-\chi^2/2v^2\} \tag{7}$$

where $v^2 = \langle \chi^2 \rangle = (R_s/V_s)^2 \langle v_r^2 \rangle$. Using equations (6) and (7) gives

$$R(k_x) = 1/v\sqrt{(2\pi)} \int_{-\infty}^{\infty} \exp\{-i(k_x\chi)\} \exp\{-\chi^2/2v^2\}\, d\chi \tag{8}$$

This integral can be looked up in stardard works of reference, giving

$$R(k_x) = \exp\{-k_x^2 v^2/2\} \tag{9}$$

Thus, the effect of the short wavelength components of range velocity is equivalent to a filter removing the shorter azimuthal components of wavelength (higher wavenumber components) from the image. The 3 db response is at $\lambda_x = 2\pi/k_x = 7{\cdot}55v$ and the half amplitude response is at $\lambda_x = 5{\cdot}33v$.

Many digitally-computed spectra from SEASAT images show what appears to be azimuthal filtering of this type figures 4 and 5).

3.4. *Calculation of the filter assuming a standard formulation for the wave spectrum*

If one knew the directional spectrum it would be possible to compute the r.m.s. range component of velocity from it knowing the radar bore-sight angles of incidence and azimuth, but there are so many parameters in such a calculation that it would be difficult to draw general conclusions. However, for satelliteborne SARs with a steep angle of incidence a major simplification is possible.

In a simple long-crested periodic wave train of amplitude a and frequency f in deep water, the water particles travel in circular orbits whose planes are in the direction of propagation of the waves. In such a wave travelling in the range direction, the plane of the circle contains the radar range direction and the radar would see an r.m.s. range velocity of $\sqrt{(2)}\pi af$. If travelling azimuthally the range component of velocity would be reduced by $\cos\theta_i$, where θ_i is the angle of incidence of the radar beam and for other directions by a factor between $\cos\theta_i$ and 1. For the SEASAT nominal value of θ_i of 20·5°, $\cos\theta_i = 0{\cdot}972$. Thus there is less than 3 per cent error involved in assuming that the r.m.s. range component of velocity is $\sqrt{(2)}\pi af$ independent of direction of travel. Using the assumption that the sea can be represented by a spectrum of component wave trains travelling independently then leads to

$$\langle v_r^2 \rangle \simeq \int_{\Omega_2}^{\Omega_1} \omega^2 S(\omega)\, d\omega \tag{10}$$

where $\omega = 2\pi f$, $S(\omega)$ is the one-dimensional spectral density of surface elevation and Ω_1 and Ω_2 are the relevant limits of integration, to be discussed later.

A commonly used formula for the one-dimensional spectrum in a fully arisen sea is the Pierson–Moskowitz spectrum (see, for example, Silvester 1974).

$$S(\omega) = (\alpha g^2/\omega^5)\exp\{-\beta(g/U\omega)^4\} \tag{11}$$

where $\alpha = 8{\cdot}10 \times 10^{-3}$, $\beta = 0{\cdot}74$ (both are dimensionless constants) and U is the wind speed at a height of 19·5 m. Putting this into equation (10) leads to

$$\begin{aligned}\langle v_r^2 \rangle &= \int_{\Omega_2}^{\Omega_1} \alpha g^2 \omega^{-3} \exp\{-\beta(g/U\omega)^4\}\, d\omega \\ &= (\alpha\sqrt{\pi}/4\beta^{1/2})U^2\{\operatorname{erf}\beta^{1/2}(g/U\omega)^2\}_{\Omega_2}^{\Omega_1}\end{aligned}$$

where erf is the error function, tabulated in standard works. Using the deep water dispersion relationship $\omega^2 = 2\pi g/\lambda$, where λ is the wavelength, gives

$$\langle v_r^2 \rangle = \frac{\alpha\sqrt{\pi}}{4\beta^{1/2}} U^2 \left[\operatorname{erf}\frac{g\beta^{1/2}}{2\pi}\frac{\lambda}{U^2}\right]_{\lambda_2}^{\lambda_1} \tag{12}$$

Putting in the numerical values for the constants (using $g = 9{\cdot}81\ \mathrm{m/s^{-1}}$)

$$\langle v_r^2 \rangle = 4{\cdot}17 \times 10^{-3} U^2[\operatorname{erf} 1{\cdot}344\,\lambda/U^2]_{\lambda_2}^{\lambda_1} \tag{13}$$

(λ in metres, U in meter per second).

$4{\cdot}17 \times 10^{-3} U^2\{\operatorname{erf} 1{\cdot}344\lambda/U^2\}$ is plotted against λ with U as a parameter in figure 3 and the limits of integration can now be considered. It will be seen that the function drops off rapidly at small wavelengths, and thus the lower limit of integration is not critical. The issue of what is the correct lower limit can therefore be avoided by integrating from zero, knowing that if, for example, the 'facets' were effectively

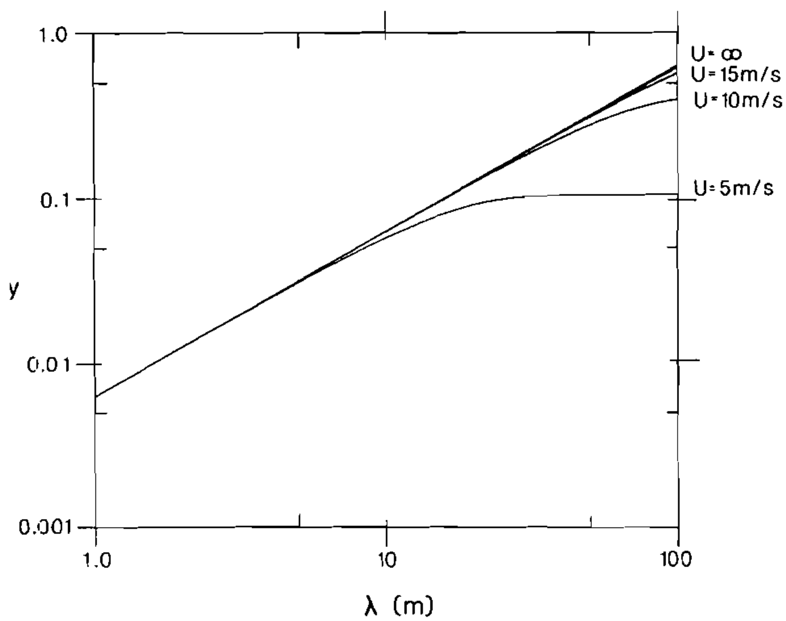

Figure 3. Plot of the function $4{\cdot}17 \times 10^{-3} U^2 \operatorname{erf}(1{\cdot}3444\lambda/U^2)$ against λ for various U.

about 1 m^2 in size, the error introduced in $\langle v_r^2 \rangle$ would be less than 5 per cent and typically more like 2 per cent with any reasonable wind speed.

Taking λ_1 as the upper limit of resolution and using the usual criterion that this is 2ρ then gives

$$\langle v_r^2 \rangle \simeq 4{\cdot}17 \times 10^{-3} U^2 \operatorname{erf}\{1{\cdot}344\, 2\rho/U^2\} \tag{14}$$

It is worth noting that since the above calculation deals with the short wavelength end of the spectrum, in most circumstances the wave energy will be characteristic of the local wind, whereas for longer waves the energy is often swell from a distant storm.

Using equation (8), the r.m.s. azimuthal offset v is given by

$$v^2 = 4{\cdot}17 \times 10^{-3} (R_s/V_s)^2 U^2 \operatorname{erf}\{1{\cdot}344\, 2\rho/U^2\}$$
$$\rightarrow 1{\cdot}265 \times 10^{-2} (R_s/V_s)^2 \rho \qquad \text{for } U^2 \gg g\rho \tag{15}$$

This asymptote corresponds to the line marked '$U = \infty$' in figure 3. These relationships can be put into equation (9) to give the aximuthal filter function.

3.5. *More general consideration of the smearing effect*

There will be occasions when a natural division occurs in the wave spectrum at the resolution limit. Examination of the Pierson–Moskowitz equation for a fully arisen sea (equation (11)) shows that there is negligible energy in wavelength components longer than approximately $\lambda = 1{\cdot}5U^2$ (SI units). For SEASAT, for example, this implies that for winds less than about 6·5 m/s, none of the locally generated wave energy can be imaged even within the nominal resolution. There may, however, be longer swell present. In general the r.m.s. velocity component due to the swell is likely to be rather small, so that an approximate value for the azimuthal filter can be calculated using the locally generated wave energy alone. There is a SEASAT image corresponding to such a case for which some relevant surface observations are available, and this will be discussed in §4.

In the more general case, equation (15) inserted into equation (9) will give a minimum value (in terms of wavelength) for the azimuthal cut-off for given local winds, and this is significant because in nearly all cases it will represent a considerable degradation of the nominal resolution.

If one were examining the effect on a known directional wave spectrum, it would be possible to iterate this process, each iteration including the r.m.s. velocity due to components cut out of the imaging by the previous calculation. This would still only give a minimum value, since it seems likely that some imaged components contribute to the smearing, but the author cannot at present see how to treat the complete problem by analytical means.

3.6. *Application to numerical simulation*

The need for numerical simulation arises because the velocity-bunching modulation can be considered as a linear problem only for long low swells. The effect of large amplitudes becomes a difficult non-linear problem for which no analytical solution is yet available (this subject is discussed by Alpers *et al.* (1981) and Hasselmann *et al.* (1984)). Thus, an understanding of the effects can only be achieved by numerical simulation of the radar imaging process using a variety of input parameters (Alpers 1983). For this it is economically important to use the coarsest possible grid, particularly for two-dimensional simulation, and since all wavenumbers in the input spectrum above the corresponding Nyquist wavenumber have to be removed, it would be desirable to be able to treat the effects of higher wavenumbers in some other way. Alpers uses a cut-off at approximately 0·25 Hz corresponding to a wavelength of approximately 25 m.

Using the theory presented above, it is possible to treat wavelengths below the limit of resolution analytically, so that only the effects of wavelengths greater than this limit need be simulated numerically, reducing the number of grid points required.

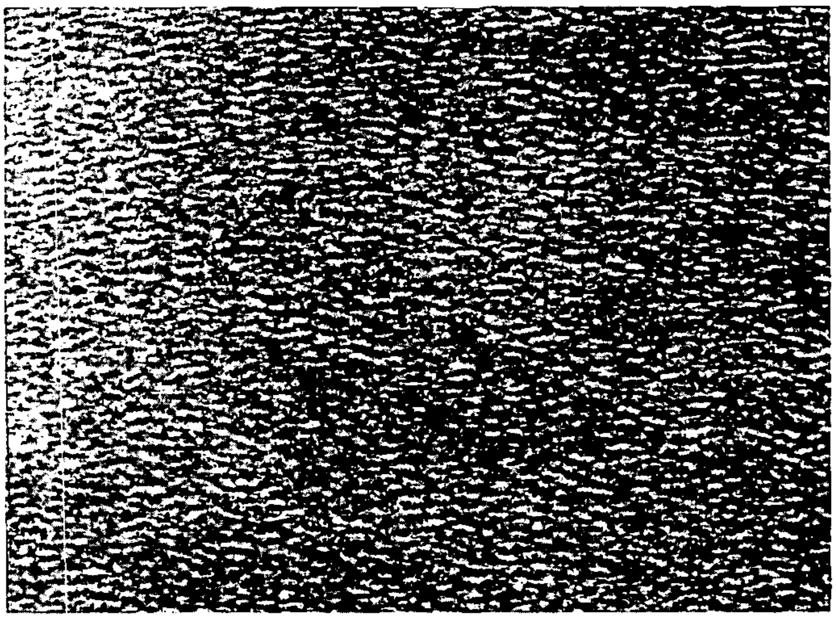

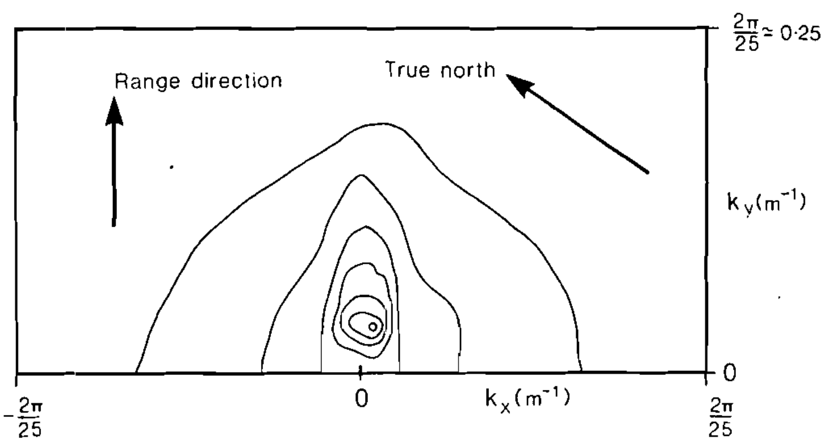

Figure 4. A SEASAT SAR scene and its Fourier transform, showing the azimuthal filtering effect. The contours are at 2:1 intervals of spectral density (for details see text).

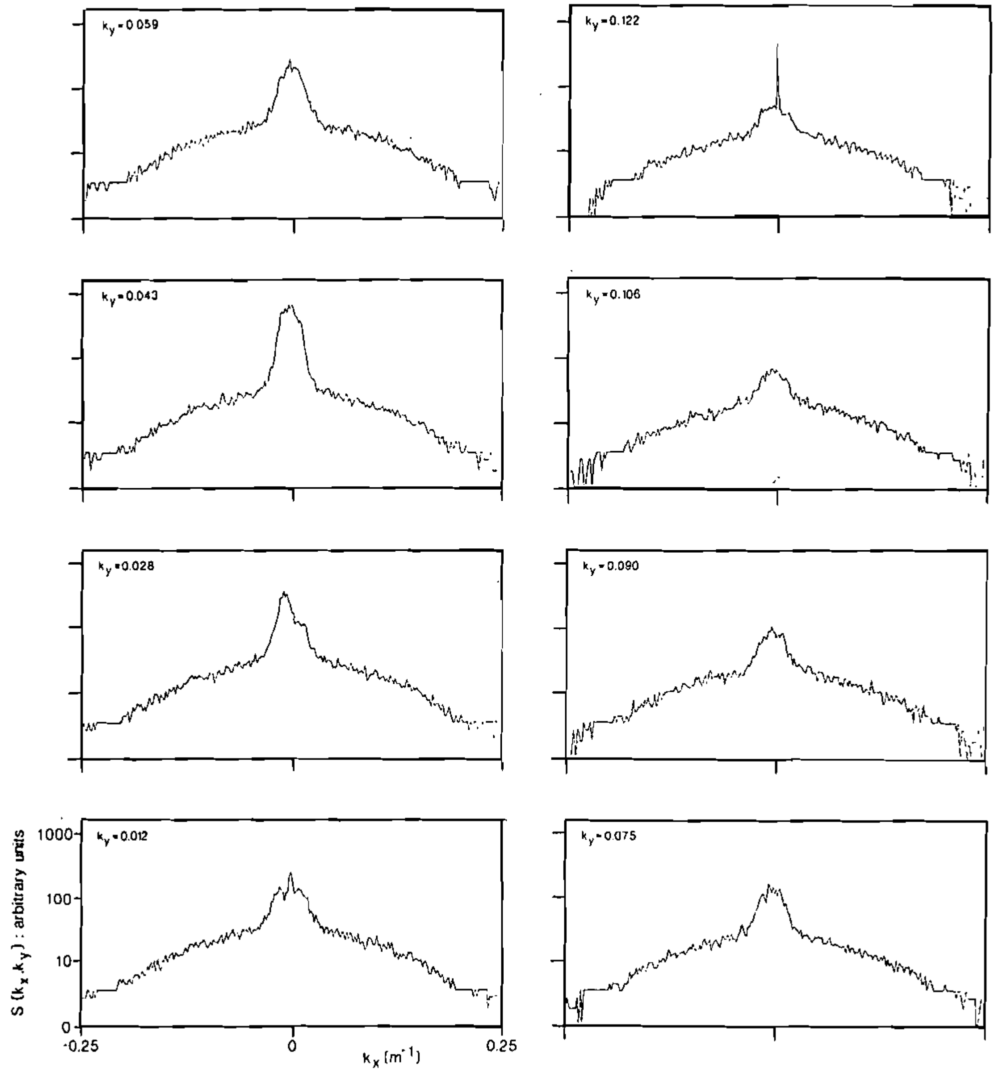

Figure 5. Eight cuts across the spectrum shown in figure 4. The plateaux visible at low spectral density correspond to the resolution intervals of the data. The spike on the spectrum of $k_y = 0{\cdot}122$ is an artefact of the analyses, and has been deleted from the spectrum shown in figure 4.

4. An example from SEASAT

At 06.50 hours on 19 August 1978 SEASAT produced an image of the sea surface at 60° 11′N and 6° 41′W. The image and its spectrum are shown in figures 4 and 5. The image data was processed digitally by the Deutsche Forschungs- und Versuchsanstalt fur Luft- und Raumfahrt e.v. (DFVLR) and received as follows:

Orbit	0762
Archive number	0523
Centre of scene	Approximately 60° 11′N, 6° 41′W
Date recorded	19 August 1978
Number of looks	4

Resolution	25 m
Scale	Amplitude of target strength
Pixel spacing	12·5 m
Image size	4050 × 4050 pixels

Figure 4 (*a*) is a 1024 × 1024 pixel subarea of the image with co-ordinates (1256, 1256) to (2279, 2279) in terms of pixel number.

Sixteen regions each 256 × 256 pixels were chosen to be Fourier transformed and the $|\text{amplitude}|^2$ of corresponding harmonics were added. A display of this power spectrum showed too much sampling variability to be readily interpretable, so it was further smoothed by a 4 × 4 running average passed over the data. The image data from DFVLR was in terms of received signal amplitude, whereas the theory outlined in this paper is in terms of backscattering cross-section, or backscattered power. For a number of reasons it was decided to transform the image as received, but since the wave modulations of the mean backscattered intensity is fairly small, the resultant errors will be second order. The processing was performed by the Marconi Research Centre under contract to the Natural Environment Research Council.

At 08.00 hours the Natural Environment Research Council's research vessel *John Murray* was at 60° 40′N and 8° 00′W and took a wind speed measurement of 6·5 m/s from 170° and a significant waveheight measurement of approximately 5 m. The ship was under way at the time so that the shipborne wave recorder gave no wave period measurement, but the visual observer estimated a swell of 10 s period with a height of about 4·5 m coming from 240° and local wind sea of about 7 s period and a height of about 2 m coming from 200°. A cold front was passing the area at the time so the wind may have been slightly variable, but the isobar spacing was about the same on both sides of the front and uniform over quite a large area of ocean in the vicinity.

The Institute of Oceanographic Sciences (IOS) also had a Waverider operating in 100 m depth of water at 60° 10′N, 2°44′W (south of Foula in the Shetland Islands). Due to Citizens Band radio interference only intermittent records were being obtained, but good quality records were obtained for 17.41 hours on 11 August and 17.41 hours on 19 August. The spectra from these are shown in figure 6 and show clearly the band of swell at approximately 10 s period. The values of H_S are considerably lower than the 5 m recorded at the *John Murray*, but with southerly winds this site has limited fetch.

Using the *John Murray* wind of 6·5 m/s and a resolution of $\rho = 30$ m, equation (14) gives $\langle v_r^2 \rangle = 0{\cdot}1758$ (m/s)^2. For the value $R_s/V_s = 115$ s for SEASAT using equations (8) and (9) gives $v = 48$ m or a 3 db azimuthal cut-off at a wavelength of 364 m, or a half amplitude cut-off at a wavelength of 257 m. It can be shown that with a satellite travelling in a curved orbit the relevant velocity is that in orbit, not that over the ground.

The image spectrum will be the product of the spectrum of the primary scattered field multiplied by the filter function, but if we make the assumption that, apart from the long-wave swell peak, the primary spectrum does not vary with direction, then figure 5 shows a fairly constant width azimuthally with a 3 db cut-off of approximately 380 m and 6 db cut-off of approximately 250 m, which is good agreement in the circumstances. (Note that the dominant wavelength of the locally generated sea would have been about 30 m for a 6·5 m/s wind).

Apart from the fact that we have some ground truth for this particular example,

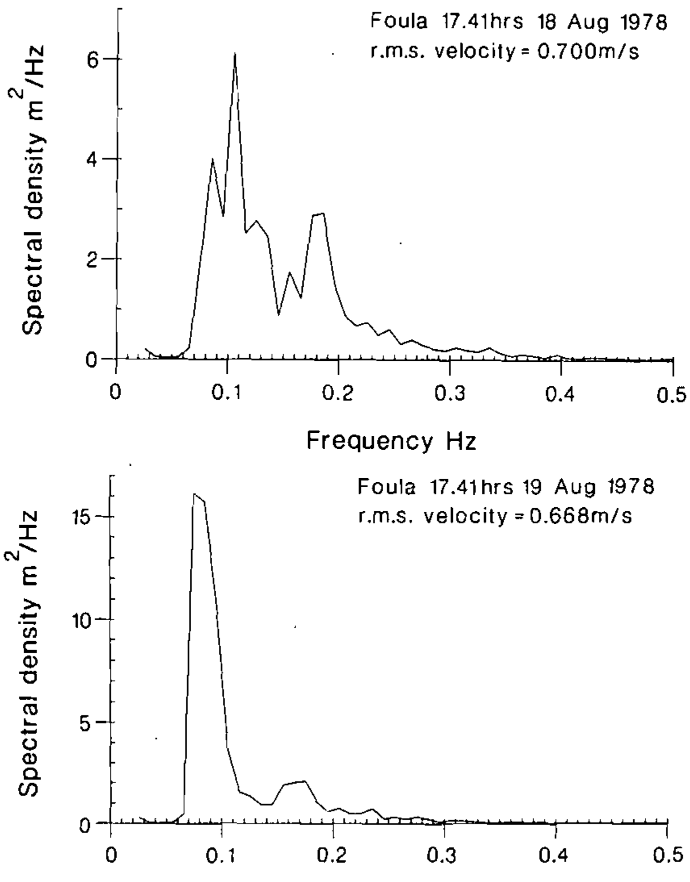

Figure 6. Wave spectra for 17.41 hours 18 August and 17.41 hours 19 August 1978. (Note the different ordinate scales.) The significant waveheights were 2·75 m and 3·21 m, respectively.

it is a relatively simple one since the modest local wind means that most of the mean-square particle velocity is contributed by components with wavelengths of less than 60 m (about two-thirds in the case of the Foula spectra shown in figure 6).

5. The effect of the phase velocity of the Bragg waves

The phase velocity of a surface wave increases with wavelength except in the capillary wave region. Some examples are

Wavelength (m)	Phase velocity (m/s)
1·0	1·249
0·25	0·626
0·10	0·401
0·04	0·272
0·02	0·233
0·01	0·248

Assuming that the waves are travelling horizontally in the range direction on an otherwise calm sea, the range component of the velocity is the above value multiplied by $\sin\theta_i$. For SEASAT $\sin\theta_i \simeq 0{\cdot}35$, so the phase velocity of the Bragg wave is 0·725 m/s, giving a range component of 0·254 m/s, corresponding to an azimuthal offset of approximately 33 m.

The Bragg wave can be travelling towards or away from the radar. If only one of these possible components is present, the whole scene will be offset by 33 m which is unimportant. If, however, it happens that an azimuthal wind is blowing so that both components are present in roughly equal amplitudes, two images will be produced offset from one another by 66 m (Alpers *et al.* 1981). This would produce cancellation of components in the spectrum with azimuthal wavelengths of approximately 132 m (Rotherham 1983). However, as calculated above, such components will already have been removed by the short wavelength smearing in all except the calmest seas, so such a minimum in the spectrum is only likely to be observed in very unusual circumstances.

For shorter wavelength radars with slower Bragg waves, the effect will be less, of course.

6. Conclusions

Based on the concept that radar backscatter can be considered as coming from 'facets', the returns from individual facets can be considered as being carried separately through the radar processor and combined into the signal just before the detector stage.

The linearity of the aperture synthesis process means that the offsets caused by velocities arising from the long and from the short wavelength parts of the spectrum can be treated independently. A convenient dividing line corresponds to the resolution limit of the radar. The effect of long wavelengths can be modelled by numerical simulation, that of short wavelengths can be treated statistically. If the computations are carried out in this order, the surface motions due to the short wavelengths produce an azimuthal smearing which has the effect of a filter which in terms of wavenumber is Gaussian low-pass, acting on the final image. For SEASAT SAR in moderate seas the cut-off wavelength is several hundred metres.

Several SEASAT images of waves show effects which can be interpreted in this way. This type of effect sets an important limitation on the utility of a satelliteborne SAR for measuring waves.

Appendix

Notation

σ	the backscattering cross-section per unit area of sea surface
σ_0	the average value of σ over an area containing many sea wavelengths
$s(x,y)=\{\sigma(x,y)-\sigma_0\}/\sigma_0$	the image intensity of an SAR scene (variation about the mean)
$s'(x,y)$	as $s(x,y)$ but after processing
$R(k_x)$	the response factor due to SAR processing
v_r	the range component of the velocity of a target
$p(v_r)$	the probability density of v_r
μ	the r.m.s. value of v_r
χ	the azimuthal offset
ν	the r.m.s. value of χ
R_s	the range of the target from the radar
V_s	the radar platform velocity
ρ	the resolution of the SAR (assumed to be the same in range and azimuth)

A_{lm}	the complex amplitude of the l,mth harmonic of a two-dimensional Fourier transform
θ_1	The angle of incidence of the radar on the sea surface
λ_1	the upper limit of the integration (sea wavelength)
k_x, k_y	the components of the sea wave number $k = 2\pi/\lambda$
$S(\omega)$	the spectral density of the sea wave system at ω
ω	2π times the frequency
$\Omega_1 \Omega_2$	limits of integration
g	the acceleration due to gravity
α	a non-dimensional constant in the Phillips and Pierson–Moskowitz spectral formulations
β	a non-dimensional constant in the Pierson–Moskowitz spectral formulation
U	the wind speed in metres per second at a height of 19·5 m above the sea surface
$\langle\,\rangle$	an ensemble average
η	the spacing of notional small pixels
$F(\mathbf{k})$	the overall system transfer function of an SAR
$G(\mathbf{k})$	the 'stationary scatter portion' of $F(\mathbf{k})$
$H(\mathbf{k})$	the moving ocean scatterer response
$J(\mathbf{k})$	the effects of the various wave imaging mechanisms

References

ALPERS, W., 1983, Monte Carlo simulations for studying the relationship between ocean wave and synthetic aperture radar image spectra. *J. geophys. Res.*, **88**, 1745.

ALPERS, W., and HASSELMANN, K., 1982, Spectral signal to clutter and thermal noise properties of ocean wave imaging synthetic aperture radars. *Int. J. remote Sensing*, **3**, 423.

ALPERS. W., ROSS, D. B., and RUFENACH, C. L., 1981, On the detectability of ocean surface waves by real and synthetic aperture radar. *J. geophys. Res.*, **86**, 6481.

BASS, F. G., FUKS, I. M., KALYKOV, A. E., OSTROVSKY, I. E., and ROSENBERG, A. G., 1968, Very high frequency radiowave scattering by a disturbed sea surface. *I.E.E.E. Trans. Antennes Propag.*, **16**, 554.

BEAL, R. C. TILLEY, D. G., and MONALDO, F. M., 1983, Large- and small-scale spatial evolution of digitally-processed ocean wave spectra from SEASAT synthetic aperture radar. *J. geophys. Res.*, **88**, 1761.

CARTWRIGHT, D. E., 1962, Waves: analysis and statistics. In *The Sea*, Vol 1, edited by M. N. Hill (New York: Interscience), Chap. 15.

GONZALEZ, F. I., BEAL, R. C. BROWN, W. E., DELEONIBUS, J., SHERMAN, J. W., III, GOWER, J. F. R., LICHY, D., ROSS, D. B., RUFENACH, C. L., and SHUCHMAN, R. A., 1979, Seasat synthetic aperture radar: ocean wave detection capabilities. *Science*, N.Y., **204**, 1418.

HASSELMANN, K., BARNETT, T. P., BOUWS, E., CARLSON, H., CARTWRIGHT, D. E., ENKE, K., EWING, J. A., GIENAPP, H., HASSELMANN, D. E., KRUSEMAN, P., MEERBURG, A., MÜLLER, P., OLBERS, D. J., RICHTER, K., SELL, W., and WALDEN, H., 1973, Measurements of wind-wave growth and swell decay during the Joint North Sea Wave Project (JONSWAP). *Dt hydrogr. Z.*, Suppl. A, **8**, No. 12.

HASSELMANN, K., RANEY, R. K., PLANT, W. J., ALPERS, W., SHUCHMAN, R. A., LYZENGA, D. R., RUFENACH, C. L., and TUCKER, M. J., 1984, Theory of SAR ocean wave imaging: the MARSEN consensus. *J. geophys Res.* (in the press).

JORDAN, R. L., 1980, The Seasat-A synthetic-aperture radar system. *I.E.E.E. J. Oceanic Engng*, **5**, 154.

KINSMAN, B., 1965, *Wind Waves* (Englewood Cliffs, New Jersey: Prentice-Hall).

OUCHI, K., 1982, Effect of random motion on synthetic aperture radar imagery. *Opt. quant. Electron.* 14, 263.

ROTHERHAM, S., 1983, Theory of SAR ocean wave imaging. In *Satellite Microwave Remote Sensing*, edited by T. D. Allan (Chichester: Ellis Horwood), Chap. 10.

SILVESTER, R., 1974, *Coastal Engineering* (Amsterdam: Elsevier), 457 pp.

TOMIYASU, K., 1978, Tutorial review of synthetic-aperture radar (SAR) with applications to imaging the ocean surface. *Proc. Inst. elect. electron. Engrs*, **66**, 563.

TUCKER, M. J., 1983, The effect of a moving sea surface on SAR imagery. In *Satellite Microwave Remote Sensing*, edited by T. D. Allan (Chichester: Ellis Horwood), Chap. 9.

WRIGHT, J. W., 1968, A new model for sea-clutter. *I.E.E.E. Trans. Antennas Propag.* **16**, 217.